Journal of The Electrochemical Society, 2021 **168** 012501
1945-7111/2021/168(1)/012501/6/$40.00 © 2021 The Electrochemical Society ("ECS"). Published on behalf of ECS by IOP Publishing Limited

Electrochemical Reduction of Copper Complexes with Glycine, Alanine and Valine

P. Pary,[1] L. N. Bengoa,[1,z] L. A. Azpeitia,[2] P. R. Seré,[1] J. M. Ramallo-López,[2] A. E. Bolzán,[2] and W. A. Egli[1]

[1]*Centro de Investigación y Desarrollo en Tecnología de Pinturas-CIDEPINT (CICPBA-CONICET-UNLP), B1900AYB La Plata, Argentina*
[2]*Instituto de Investigaciones Fisicoquímicas Teóricas y Aplicadas-INIFTA (CONICET-UNLP), La Plata, Bs. As., Argentina*

Basic electrochemical studies of coordination complexes between cupric ions and simple amino acids as ligands (L), namely glycine, alanine and valine, have been carried out to provide insight in the effect of complexation on Cu^{2+} discharge electrochemistry. The results show that there are strong differences in their cyclic voltammograms, despite the similarities in coordination equilibrium, central atom *d* electronic structure and inner sphere coordination distances (verified by chemical equilibrium quantification, UV spectroscopy and EXAFS). Evidence of mass transport limitations by diffusion of the neutral CuL_2 complexes in solution, and cuprous species generation on the electrode during copper electrodeposition was found, both of which proved to be the main phenomena accounting for the different electrochemical behaviour previously mentioned. Voltammetric studies also showed that, surprisingly, cuprous species are produced not only at the onset of copper electroreduction but at more cathodic potentials. Furthermore, results suggest the existence of a cuprous compound layer beneath the metallic copper deposit. The data gathered in this investigation, leads to the conclusion that the bigger molecular size and organic nature of the ligands induce unexpected processes on the copper electroreduction mechanism.
 [DOI: 10.1149/1945-7111/abd92b]

Manuscript submitted November 12, 2020; revised manuscript received December 18, 2020. Published January 18, 2021.

Coordination complexes formed between copper and nitrogen bearing ligands have been intensely investigated for more than a hundred years. Transition metals interaction with biological systems is one of the main phenomena that has driven this work. Early publications in this topic by Ley[1] were focused on the chemical reactions of Cu^{2+} ion in aqueous solution with simple amino acids, which were later used as simple models to understand the real behaviour of more complex biological systems.[2–5] The basic ligands included in those works were generally glycine, alanine and other natural α-amino acids. As more advanced experimental techniques were available, more complex formulations appeared, e.g., other types of amino acids with various functional chemical groups naturally occurring in living organisms,[6] their mixtures[7,8] and higher molecular weight species that resemble biological proteins such as polyglutamic acid[9,10] and other peptides.[11] Recent publications in this field confirm the increasing interest in this topic, still growing to present days, in several fields including drug delivery and medical applications.[12–16] Copper amino acid complexation interaction has received some attention in metal pick up by soil and minerals in nature as well.[17] Another line of work that has been increasing its activity in the last decades is in the field of electrochemical science, mainly related with metal electrodeposition.[18–28] Some authors have dealt with amino acids as additives in copper electrodeposition[22,23] and others have used them as main components in their electrolytes.[26–28] Although glycine has been the most investigated species due to its simple molecular structure, other amino acids have also been considered. Several variables have been studied, including pH, amino acid-copper concentrations ratio and current density, among others, and numerous instrumental techniques have been utilized to understand the influence of the molecular structure of the copper complexes on the mechanism of copper electroreduction in presence of these organic compounds. In particular, Survila et al. have published several articles about copper electrodeposition in the presence of different types of amino acids, giving special attention to the cuprous oxide layer that forms during the electroreduction of this metal.[19,20,22,24,29]

In this work, the electrochemical behaviour, and some physicochemical properties of three copper complexes with simple α amino acids presenting slight differences in their molecular structure (glycine, alanine and valine), were studied. The aim of the investigation is to give some fundamental experimental data to contribute to the understanding of the interaction between copper ions and these organic ligands and their effect on metal electrodeposition.

Experimental

Solutions containing 0.005 mol l^{-1} $CuSO_4.5H_2O$ (Cicarelli RG, 99%) + 0.05 mol l^{-1} of either glycine (GlyH), L-alanine (AlaH) or L-valine (ValH) (all Anedra RG) and 0.10 mol l^{-1} of $NaClO_4$, (supporting electrolyte) were prepared using high resistivity (>18 MΩ) osmosis water. The pH was then adjusted to 8 by small additions of KOH (Anedra RG 99%).

Equilibrium simulations were performed using the RStudio software, following a calculation procedure similar to the one used by Ballesteros et al.[30] based on the complexation coefficient concept. Acid-based, formation and precipitation constants used in this work were taken from literature.[31,32]

Cyclic voltammetry (CV) experiments were conducted using an Autolab PGSTAT 204 potentiostat/galvanostat controlled by Nova 2.1 software using a standard three-electrode cell. A glassy carbon rotating disc electrode (0.04 cm^2) was used as working electrode, a copper wire as counter electrode and a saturated silver chloride electrode (SSC) as the reference electrode. All the potentials in the text are referred to the SSC scale. The electrode potential was swept between −1.0 V and 0.50 V at different scan rates (ν, $V{\cdot}s^{-1}$) with and without rotation of the working electrode. Cathodic potential steps were also applied to the glassy carbon electrode (0.04 cm^2) for 10 s using the same experimental set-up. Temperature in the cell was kept at 30 °C using a FRIGOMIX 1495 thermostat.

UV–Visible absorbance spectra of the three electrolytes were recorded in the range from 200 nm to 900 nm using a UV 2600 Shimadzu spectrophotometer (5.0 slit width, 0.1 s accumulation time) at 25 °C.

EXAFS experiments at the Cu K edge (8979 eV) were performed using a RIGAKU R-XAS Looper spectrometer in transmission mode. An ionization chamber filled with Ar was used to measure the incident radiation and a solid-state detector to measure the transmitted intensity. Aqueous electrolytes were placed in sample holders with kapton windows. The energy calibration was done using a foil of metallic cooper. The quantitative analysis of the results was carried out using the IFFEFIT package.[33] Structural

[z]E-mail: l.bengoa@cidepint.ing.unlp.edu.ar

information around the absorbing atom, including coordination numbers, interatomic distances, and their Debye-Waller factors (σ^2), were obtained from Artemis using a nonlinear least squares fit of the Fourier transformed data in r-space, with theoretical amplitudes and phase shifts for all single scattering paths calculated by FEFF.[34] All data fits were made for the range 1.0–2.0 Å in the r-space and generated by Fourier filtering the k^2-weighted EXAFS over the 2–11 $Å^{-1}$ range in the k-space with a Hanning window. The theoretical scattering path amplitudes and phase shifts used in these fits were calculated from the reported structures of a $Cu(L\text{-glutamic})_2$ complex.[16] Passive reduction factor was obtained from single scattering fits of the EXAFS spectra of the metal foil by constraining the coordination number to 12.

Rotating ring disk electrode (RRDE) runs were recorded using a Tacussel rotating Pt-disk/Pt-ring electrode, with a disk geometric area of 0.12 cm^2, and collection efficiency N = 0.24, were N is defined as,[35]

$$N = \frac{I_R}{I_D}\frac{n_D}{n_R}$$

Being I_R and I_D, the currents measured at the ring and at the disk, respectively, n_R and n_D the number of electrons transferred in the ring and the disk electrode reactions, respectively.

RRDE experiments were performed using an Autolab 128 N that included a bipotentiostat (BA) module, allowing simultaneous control of the potential of the disk (E_D) and the ring (E_R).For CV and RRDE, electrode rotation speed (ω) was varied from 1000 to 4000 rpm by means of a Radiometer CVT101 speed controller.

Results and Discussion

Figure 1 shows the chemical structure of the three amino acids included in this investigation. The molecular weight increment in the sequence GlyH, AlaH and ValH is the smallest possible in the naturally occurring α amino acid series. In aqueous solution these compounds present two acid base equilibria (k_1 and k_2 in Table I) corresponding to the carboxylic acid and to the amino protonation reactions, respectively. When cupric ion is present in solution several additional chemical equilibria appear, as shown in Fig. 2 for the copper glycine system.

For pH between 3 and 11 the main chemical equilibria present in solution can properly be described by the following chemical reactions,

$$Cu^{2+} + L^- \rightleftharpoons CuL^+ \; K_1 \qquad [1a]$$

$$Cu^{2+} + 2L^- \rightleftharpoons CuL_2 \; K_2 \qquad [1b]$$

Where L stands for the amino acid ligand and K_1 and K_2 are the equilibrium constants for each equation (Table I).

As it can be deduced from the quantitative information presented in Table I, it sounds quite reasonable to expect a similar behaviour of the copper complexes produced with the three amino acids in solution. This was confirmed by simulation of the speciation equilibria for the three copper complexes (not shown), which yielded identical results to those for the copper glycine case (Fig. 2). For the specific case of pH = 8, any of the three amino acids forms a neutral simple CuL_2 soluble complex species with the copper ions, following reaction pathway 1.

Figure 3 shows the CV profiles for the three soluble copper complexes in quiescent conditions. The two anodic peaks at −0.20 V (peak I_a) and +0.15 V (peak II_a) correspond to the anodic dissolution of copper through a two-step mechanism that has already been reported for several copper amino acid complexes elsewhere.[27,36,37] Peak II_a is related to the anodic dissolution of the copper film produced on the GC surface. From the integration of this peak it results evident that less copper is deposited as the molecular weight of the ligand increases. Regarding the cathodic scans, small

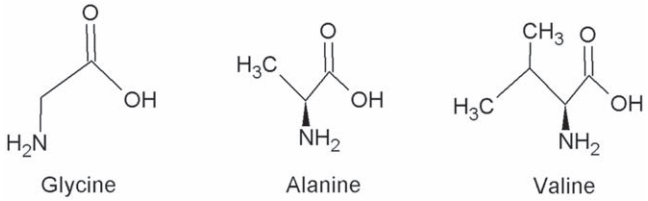

Figure 1. Chemical structure of amino acids.

differences in the limiting curent for copper electrodeposition were observed, in the potential range from −0.40 V to −1.10 V, for the three amino acids considered, which may be indicative of changes in the diffusion coefficient with the size of the ligand. Therefore, rotation speed of the RDE was varied from 100 rpm to 500 rpm and the value of current at −0.6 V was registered. From the corresponding Koutecky-Levich plots the following diffusion coefficients were obtained for the soluble complex CuL_2 species (Table II). Despite the fact that similar D values can be found in literature for copper glycine complexes,[18] the variation in this parameter observed for different aminoacids does not correlate with the small changes in cathodic limiting current. For example, based on our measurements $Cu(Gly)_2$ present a D value 50% larger that $Cu(Ala)_2$ complexes, which according to Levich equation should lead to an increase of 30% in limiting current (assuming that electrolyte viscosity and density does not vary significantly). However, the recorded values (Fig. 3) showed only a 7% higher limiting current for the $Cu(Gly)_2$ system. The latter suggests that there are other processes not related to mass transport involved in the electrochemical response of Cu-aminoacids solutions.

When the electrode was rotated at 1000 rpm (Fig. 4) a tenfold increase in currents was observed and the first anodic peak almost disappeared, as previously reported for the copper-glutamic acid system,[27] and the difference in the second peak area was more accentuated between the three amino acids than for static conditions. Looking at the cathodic sweeps in Fig. 4, large differences in cathodic currents arise due to electrode rotation. This behaviour could be attributed to the existence of a soluble Cu^+ intermediate,[27] which is generated in the three electrolytes considered but at different rates. Under static conditions, the intermediate remains in the vicinity of the electrode readily available for its subsequent reduction. In contrast, when the electrode is rotated, soluble species are removed from the disk surface due to shear forces, which in turn leads to a decrease in the deposition current density of the CuAla and CuVal electrolytes. Evidence in support of this idea was found using a RRDE (see following paragraphs), which also showed that the amount of Cu^+ intermediate is higher for the CuGly system. The latter would also explain the changes in D observed, since the existence of this intermediate has a direct impact on the effect that electrode rotation has on cathodic current density.

In order to search for differences between the copper complexes and to explain the differences observed in electrochemical behaviour depicted in Figs. 3 and 4, their UV–visible absorption spectra were recorded (Fig. 5). It should be noticed that absorption bands in the range 200–370 nm, which can be assigned to $n \rightarrow \pi^*/\pi \rightarrow \pi^*$ intraligand transitions associated to the amino acid molecules, are excluded from the spectra for clarity. All soluble complexes exhibit one low intensity absorption peak in the visible region with an absorption maxima located around 630 nm,[38–40] being the copper glycine complex at the low energy side and valine at the high energy end. These results show that the "*d*" electronic structure of the central copper ion in the three complexes is very similar and their small crystal field energy splitting differences could be explained assuming some increasing inductive effect from the organic ligands accordingly to their molecular size.

X-ray absorption spectra at the Cu K-edge were registered for the three electrolytes (Fig. 6) and the EXAFS oscillations were analysed to identify eventual differences in the first coordination sphere of Cu

Table I. Constants for L acid base equilibria and CuL_2 formation.

	L Acid/Base Equilibrium Constants		CuL_2 Formation Constants	
	log k_1	log k_2	log K_1	log K_2
Gly	2.36 ± 0.04	9.56 ± 0.02	8.12 ± 0.06	15.0 ± 0.1
Ala	2.31 ± 0.04	9.71 ± 0.02	8.11 ± 0.05	14.9 ± 0.1
Val	2.26 ± 0.02	9.49 ± 0.03	8.09 ± 0.04	14.9 ± 0.1

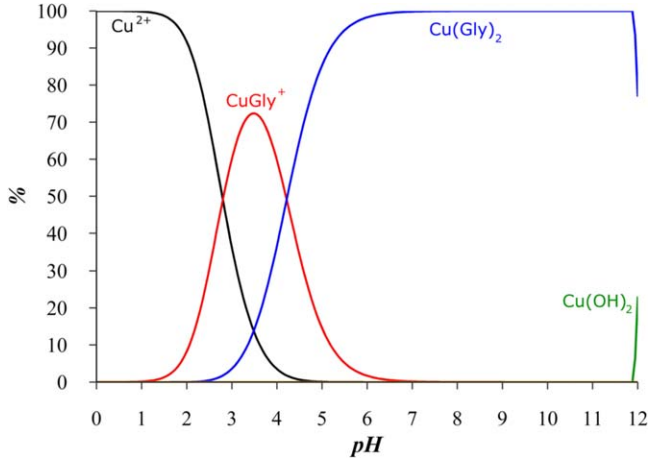

Figure 2. Speciation equilibrium diagram for copper-glycine complexes (30 °C).

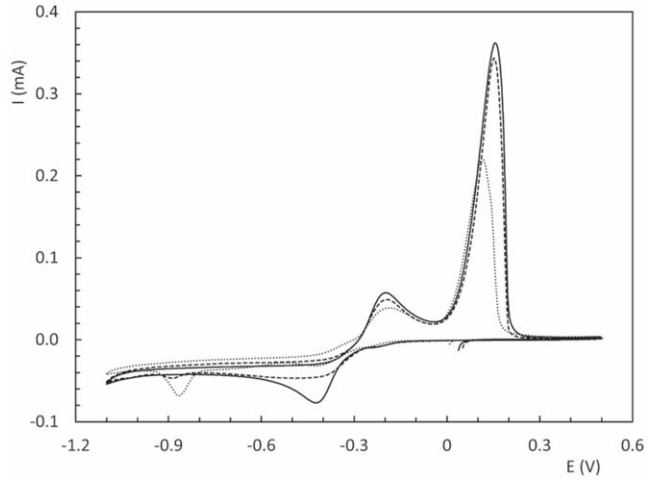

Figure 3. CV curves in static conditions, $Cu(Gly)_2$ (——), $Cu(Ala)_2$ (- - -) and $Cu(Val)_2$ (••••••). (30 °C, 0.02 Vs^{-1}).

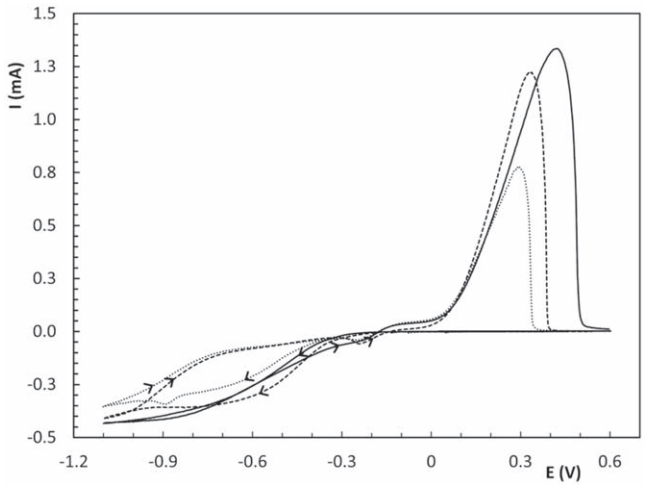

Figure 4. CV curves for copper complexes at 1000 rpm. $Cu(Gly)_2$ (——), $Cu(Ala)_2$ (- - -) and $Cu(Val)_2$ (••••••). (30 °C, 0.02 Vs^{-1}).

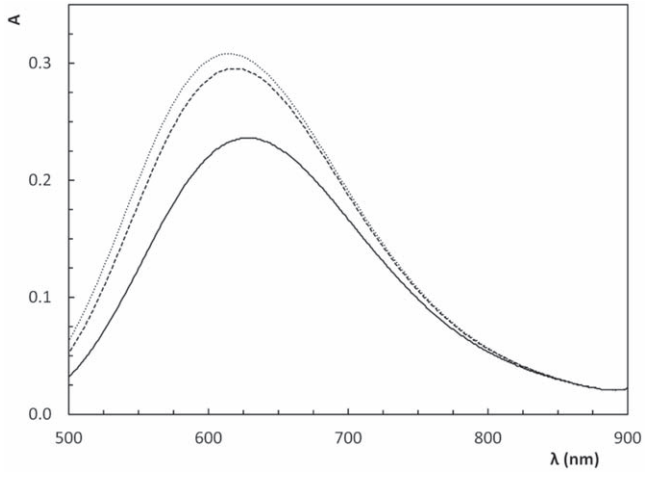

Figure 5. UV–visible spectra for three CuL_2 complexes (500 to 900 nm shown only). $Cu(Gly)_2$ (——), $Cu(Ala)_2$ (- - -) and $Cu(Val)_2$ (••••••).

Table II. Diffusion coefficients of CuL_2 complexes.

Complex	D (cm^2s^{-1}) × 10^6
$Cu(Gly)_2$	2.4
$Cu(Ala)_2$	1.6
$Cu(Val)_2$	1.3

atoms in the complexes. Fitting results are shown in Table III and confirm that the first coordination sphere around Cu atoms in the three complexes are almost identical. Results are compatible with previous work reported for similar compounds.[41] Coordination number and interatomic distances of first neighbours are very similar and compatible with the smooth induction effect depicted for the UV-visible spectra. It is worth noting that the complexes are slightly more compact for the heavier ligands.

Figure 7 shows the RRDE first cathodic sweep recorded at $v = 0.02$ Vs^{-1} and $w = 4000$ rpm, between -1.20 V and $+0.50$ V corresponding to each amino acid-containing solution. In the case of CuGly electrolyte the anodic limit must be set at $+0.70$ V to allow complete dissolution of metallic copper. Thus, the disk current (I_D) confirms the higher copper electrodeposition rate as the molecular weight of the amino acids decreases. Experiments varying E_R from -0.20 V to $+0.50$ V were made (curves not shown) and based on

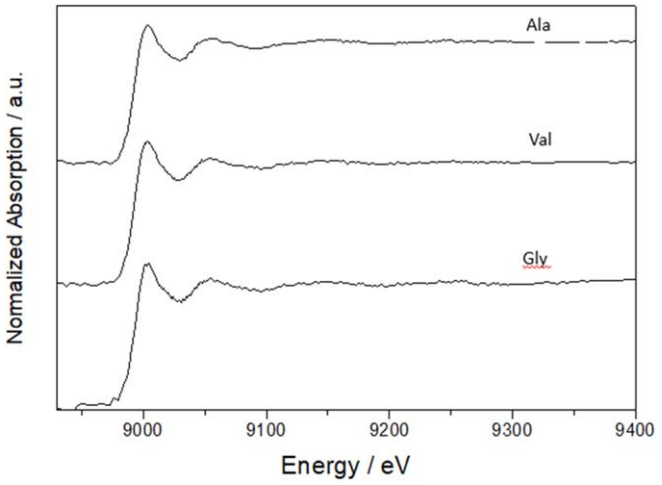

Figure 6. Normalized X-ray absorption spectra around the copper K-edge for the three complexes.

Table III. Fitting results of EXAFS spectra for copper complexes with amino acids (O/N neighbours).

Sample	Coordination Number	Distance (Å)	σ^2 (Å^2)
$Cu(Gly)_2$	3.9 ± 0.4	1.98 ± 0.03	0.0011 ± 0.0007
$Cu(Ala)_2$	4.0 ± 0.4	1.94 ± 0.05	0.0027 ± 0.0007
$Cu(Val)_2$	3.8 ± 0.4	1.95 ± 0.04	0.0030 ± 0.0007

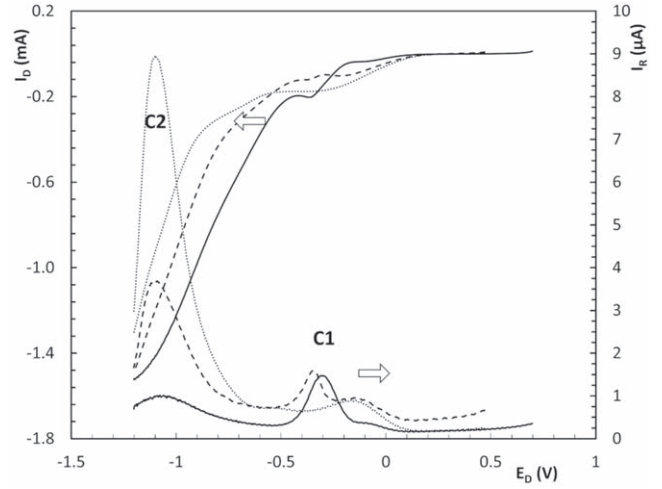

Figure 7. I_D and I_R during RRDE cathodic sweep for $Cu(Gly)_2$ (——), $Cu(Ala)_2$ (- - -) and $Cu(Val)_2$ (••••••) at 4000 rpm. (30 °C, 0.02 Vs^{-1}).

those results, E_R was then set at +0.50 V for the following runs in order to oxidize Cu^+ and avoid the Cu^{2+} electroreduction reaction interference. Looking at ring's current response (I_R), two anodic peaks arise. One smooth shallow peak (C1) in the −0.20 V−−0.40 V electrochemical potential window and C2 at more cathodic potentials (−1.1 V). C1 is very similar for the three CuL_2 complexes and C2 is strongly dependent on the chemical nature of L, being quite smaller for $Cu(Gly)_2$ and increases practically tenfold its magnitude for $Cu(Val)_2$. This behaviour could be responsible of the shoulder CuVal present in the CV cathodic sweep at ≈−1.0 V (Fig. 4), negligiblet in CuAla and absentin CuGly.

Based on this evidence and previous studies, C1 can be associated with Cu^+ oxidation at the ring.[27] In the case of C2

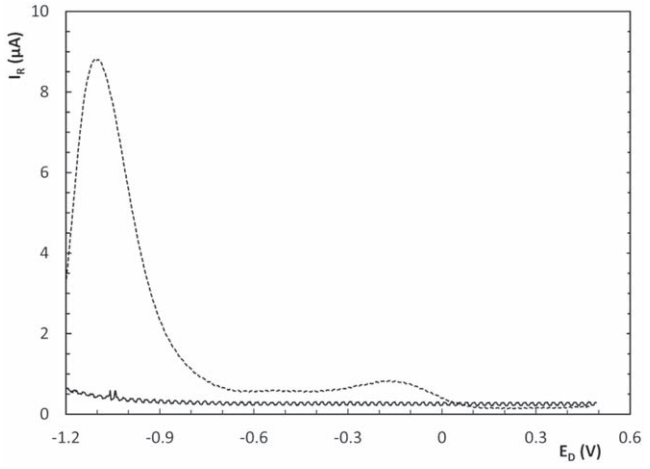

Figure 8. I_R cathodic sweep of RRDE CV for $Cu(Val)_2$ and valine without copper in solution (at 4000 rpm, 30 °C, 0.02 Vs^{-1}).

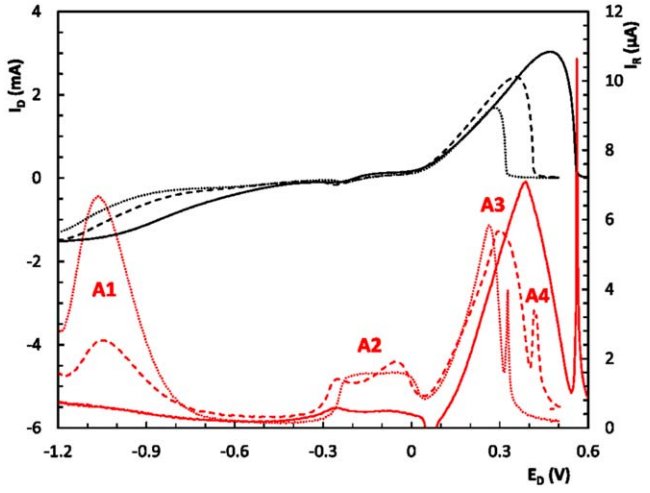

Figure 9. I_D (black curves) and I_R (red curves) for the anodic sweep of the RRDE curves for $Cu(Gly)_2$ (——), $Cu(Ala)_2$ (- - -) and $Cu(Val)_2$ (••••••), at 4000 rpm. (30 °C, 0.02 Vs^{-1}).

both, proton electroreduction and amino acids side reactions at the disc, must be discarded because it appears at an unexpected high cathodic potential. Figure 8 shows the RRDE cathodic sweeps for valine solutions with and without copper ions. As it can be seen, C2 is present only when Cu^{2+} is in solution indicating that I_R is caused by Cu^+ oxidation and not by other process taking place at the disk. The same behaviour was found for glycine and alanine electrolytes (not shown).

Figure 9 shows the RRDE response corresponding to the voltammetric positive sweep at the disc obtained after reaching the negative switching potential, as shown in Fig. 7. At the ring, A1 peaks reproduce the same behavior of peak C2 during the negative sweeps, suggesting that an electrochemical process producing Cu^+ soluble species takes place at the disk in this potential window, regardless of the sweeping direction, which are collected at the ring. In contrast, in the potential range corresponding to C1, A2 peaks appear at slightly different potential values and with a splitting tendency. This suggest that Cu^+ is produced at the electrode on the onset of copper electro reduction during the cathodic sweep and when metallic copper starts to dissolve at the anodic cycle. For potentials more positive than 0.05 V a large and wide current peak (A3) appears for the three electrolytes. Peak A3 appears in the same potential range corresponding to the anodic current peaks related to the electro dissolution of the copper layer at the disc, indicating that

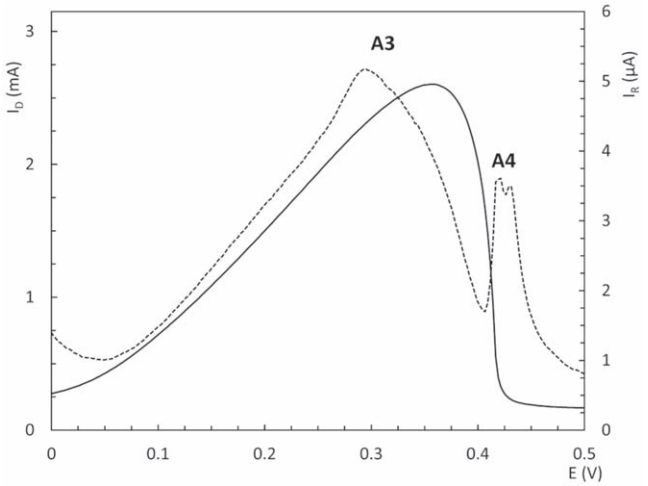

Figure 10. I_D (——) and I_R (- - -) detail for A3 and A4 peaks of the anodic sweep of RRDE curves for $Cu(Ala)_2$ electrolyte, at 4000 rpm. (30 °C, 0.02 Vs^{-1}).

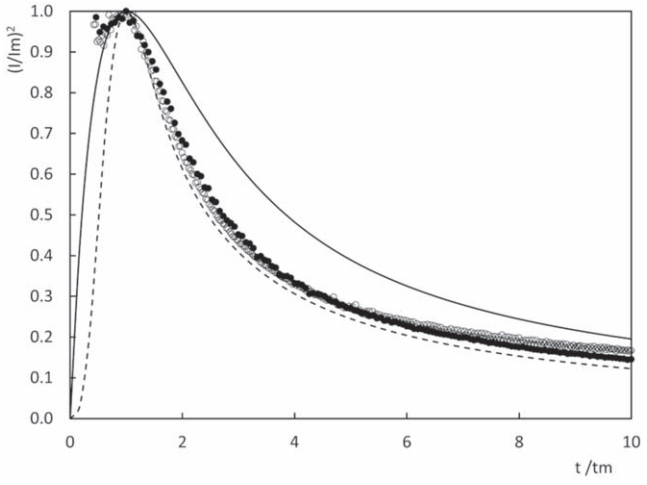

Figure 12. Non-dimensional plots of the transients for $Cu(Gly)_2$ (●) at E = −0.60 V and $Cu(Ala)_2$ (○) at E = −0.65 V.

the latter consists in a two steps mechanism involving a soluble Cu^+ species. The differences observed for the three aminoacids could be ascribed to changes in the stability of Cu^+ species. Based on the reported data,[42] it could be assumed that as the molecular size of the aminoacid increases the stability of Cu^+ complexes decreases. This would shift the redox potential of the couple Cu^{2+}/Cu^+ to more cathodic potentials, explaining the large peak C2 observed for valine, and why it was the practically absent in glycine containing electrolyte (Fig. 7). However, since there is little information available about Cu^+-aminoacids complexes, it is impossible to verify this postulate and will be investigated in detail in the future.

A quite interesting fact is the very thin and sharp current peak (A4) observed immediately after peak A3. Figure 10 shows a detail of A3 and A4 peaks at the ring, together with I_D profile for the $Cu(Ala)_2$ complex. It is clearly seen that when bulk metallic copper finishes its anodic dissolution, another soluble species leaves the disc and is detected at the ring. As it can be observed in Fig. 9, peak A4 always appears after the complete dissolution of metallic copper for the three CuL_2 complexes. I_D being zero when peak A4 appears, suggests that there is a thin layer of Cu^+ compound in the interface between copper and Pt that chemically dissolves after metallic copper is stripped away. This phenomenon, however, requires further investigations.

Electrode current responses to potential steps within the potential range corresponding to the copper electrodeposition process were measured to determine the nucleation and growth mechanism of copper deposition from the three electrolytes under study. Current transients for different negative potentials are shown in Fig. 11. For glycine and alanine, a typical current maximum[43] that moves to shorter times as the potential is made more negative, appears. For the $Cu(Val)_2$ complex, the current transients exhibit only a diffusion current decay without a current maxima.[44] This behaviour is coherent with D values shown in Table II. For glycine- and alanine-containing solutions, Scharifker models of nucleation and growth processes were evaluated and the results suggest a 3D progressive nucleation and growth mechanism. Non-dimensional current ($(I/I_m)^2$) vs non-dimensional time (t/t_m) plots for $Cu(Gly)_2$ and $Cu(Val)_2$ transients are shown in Fig. 12 for specific potential steps values.

Conclusions

Cupric ions form stable soluble complexes with simple α-amino acids. They have identical chemical speciation behaviour in solution and their UV absorption and EXAFS spectra suggest that they have also comparable inner coordination structures. Some differences, however, appear in their electrochemical behaviour, as shown by the voltammograms run in both quiescent and rotating electrode conditions, partially due to diffusion limitations at strong cathodic polarization. This is evidenced from their different diffusion coefficients values. This is quite reasonable based on the different molecular volume of amino acids considered in this study. Nucleation and growth current maxima in the potentiostatic current transients are gradually depressed due to diffusional effects as the ligand size increases, confirming this tendency in the series glycine, alanine and valine. In the present work, strong evidence is presented relating to the generation of soluble cuprous species at the onset of metallic copper deposition and at more negative potentials, before the hydrogen evolution reaction takes place. These phenomena, together with limitations for cupric ions diffusion towards the electrode surface, inhibits metallic copper electrodeposition. We also confirm, as other authors had proposed, that cuprous ions are produced during the anodic stripping of the electrodeposited copper

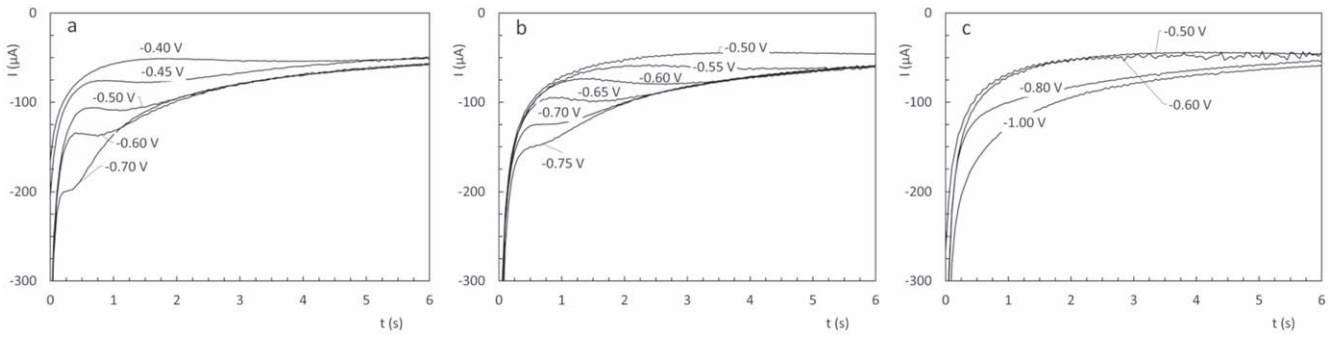

Figure 11. Current transients for (a) $Cu(Gly)_2$, (b) $Cu(Ala)_2$ and (c) $Cu(Val)_2$.

layer. Another interesting finding is the detection of a thin layer of a cuprous compound, possibly an oxide, underneath the metallic copper deposit. This layer is chemically dissolved when the copper deposit is anodically stripped away. This subject is currently under investigation.

Acknowledgments

This work was financially supported by the Agencia Nacional de Promoción Científica y Tecnológica of Argentina, the Consejo Nacional de Investigaciones Científicas y Técnicas (CONICET) and the Comisión de Investigaciones Científicas de la Provincia de Buenos Aires (CICPBA). The authors would also like to thank the and Universidad Nacional de La Plata (UNLP) for the funds and support provided for this investigation.

ORCID

L. N. Bengoa https://orcid.org/0000-0002-0608-8248

References

1. H. Ley, *Zeitschrift für Elektrochemie und angewandte physikalische Chemie*, **10**, 954 (1904).
2. P. Kober and K. Sugiura, *J. Biol. Chem.*, **13**, 1 (1912).
3. H. Borsook and K. V. Thimann, *J. Biol. Chem.*, **98**, 671 (1932).
4. N. C. Li and E. Doody, *JACS*, **76**, 221 (1954).
5. N. C. Li, J. M. White, and R. L. Yoest, *JACS*, **78**, 5218 (1956).
6. B. A. Goodman, D. B. McPhail, and H. K. J. Powell, *J. Chem. Soc., Dalton Trans.*, **3**, 822 (1981).
7. T. Sakurai, O. Yamauchi, and A. Nakahara, *Bull. Chem. Soc. Jpn.*, **51**, 3203 (1978).
8. S. Shah, K. Suyan, and C. Gupta, *Talanta*, **27**, 455 (1980).
9. H. Takesada, H. Yamazaki, and A. Wada, *Biopolymers: Original Research on Biomolecules*, **4**, 713 (1966).
10. K. Yamaoka and T. Masujima, *Bull. Chem. Soc. Jpn.*, **52**, 1286 (1979).
11. B. de Castro, J. F. Lima, and S. Reis, *J. Pharm. Biomed. Anal.*, **13**, 465 (1995).
12. S. Awasthi, *Cryst. Res. Technol.*, **50**, 304 (2015).
13. G. Valora, R. P. Bonomo, and G. Tabbì, *Inorg. Chim. Acta*, **453**, 62 (2016).
14. T. V. Berestova, L. G. Kuzina, N. A. Amineva, I. S. Faizrakhmanov, I. A. Massalimov, and A. G. Mustafin, *J. Mol. Struct.*, **1137**, 260 (2017).
15. L. Hernández, E. Del Carpio, W. Madden, G. Lubes, A. Perez, R. E. Rodríguez-Lugo, V. R. Landaeta, M. L. Araujo, J. Daniel Martínez, and V. Lubes, *Physics and Chemistry of Liquids*, **58**, 31 (2018).
16. M. S. Bukharov, V. G. Shtyrlin, A. S. Mukhtarov, G. V. Mamin, S. Stapf, C. Mattea, A. A. Krutikov, A. N. Il'in, and N. Y. Serov, *Phys. Chem. Chem. Phys.*, **16**, 9411 (2014).
17. W. t. Bodenheimer and L. Heller, *Clay Miner.*, **7**, 167 (1967).
18. A. Survila and V. Uksiené, *Electrochim. Acta*, **37**, 745 (1992).
19. A. Survila, P. Kalinauskas, and V. Uksiené, *Electrochim. Acta*, **38**, 2733 (1993).
20. A. Survila, P. Kalinauskas, E. Ivaškevič, and W. Kutner, *Electrochim. Acta*, **42**, 2935 (1997).
21. V. Kublanovsky and K. Litovchenko, *J. Electroanal. Chem.*, **495**, 10 (2000).
22. A. Survila, *J. Electroanal. Chem.*, **501**, 151 (2001).
23. A. Bolzán, *Electrochim. Acta*, **113**, 706 (2013).
24. S. Aksu and F. M. Doyle, *J. Electrochem. Soc.*, **148**, B51 (2001).
25. A. Survila, A. Survilienė, S. Kanapeckaitė, J. Büdienė, P. Kalinauskas, G. Stalnionis, and A. Sudavičius, *J. Electroanal. Chem.*, **582**, 221 (2005).
26. J. Ballesteros, E. Chaînet, P. Ozil, G. Trejo, and Y. Meas, *J. Electroanal. Chem.*, **645**, 94 (2010).
27. P. Pary, L. N. Bengoa, and W. A. Egli, *J. Electrochem. Soc.*, **162**, D275 (2015).
28. G. O'Connor, K. Lepkova, J. Eksteen, and E. Oraby, *Hydrometallurgy*, **181**, 221 (2018).
29. A. Survila, *Electrochemistry of Metal Complexes: Applications from Electroplating to Oxide Layer Formation* (John Wiley & Sons, New York) (2015).
30. J. Ballesteros, E. Chaînet, P. Ozil, G. Trejo, and Y. Meas, *Electrochim. Acta*, **56**, 5443 (2011).
31. M. Pourbaix, *Atlas of Electrochemical Equilibria in Aqueous Solutions* (National Association of Corrosion Engineers, Houston, Texas, USA) p. 644 (1974).
32. R. M. Smith and A. E. Martell, *Critical Stability Constants: Second Supplement* (Springer, Berlin) (1989).
33. B. Ravel and M. Newville, *J. Synchrotron Radiat.*, **12**, 537 (2005).
34. S. Zabinsky, J. Rehr, A. Ankudinov, R. Albers, and M. Eller, *Physical Review B*, **52**, 2995 (1995).
35. A. J. Bard and L. R. Faulkner, *Fundamentals and Applications* (Wiley, New York) p. 482 (2001).
36. X.-L. He and J.-B. He, *Electrochim. Acta*, **169**, 90 (2015).
37. J. Ballesteros, L. Torres-Martínez, I. Juárez-Ramírez, G. Trejo, and Y. Meas, *J. Electroanal. Chem.*, **727**, 104 (2014).
38. M. M. Darj and E. R. Malinowski, *Anal. Chem.*, **68**, 1593 (1996).
39. A. Stanila, A. Marcu, D. Rusu, M. Rusu, and L. David, *J. Mol. Struct.*, **834**, 364 (2007).
40. K. Hayase and R. G. Zepp, *Environmental Science & Technology*, **25**, 1273 (1991).
41. P. D'Angelo, E. Bottari, M. Festa, H.-F. Nolting, and N. Pavel, *The Journal of Physical Chemistry B*, **102**, 3114 (1998).
42. A. Martell and R. Smith, *Critical Stability Constants, Vol. 1: Amino Acids* (Springer , New York) 1st ed. (1974).
43. B. R. Scharifker and J. Mostany, *J. Electroanal. Chem. Interfacial Electrochem.*, **177**, 13 (1984).
44. D. Mazaira, C. Borrás, J. Mostany, and B. Scharifker, *J. Electroanal. Chem.*, **631**, 22 (2009).